A MULTISTAGE TIME-STEPPING SCHEME FOR THE THIN-LAYER NAVIER-STOKES EQUATIONS

R. C. Swanson, Jr.
NASA Langley Research Center
Hampton, Virginia

Eli Turkel
Tel Aviv University
Tel Aviv, Israel

V. N. Vatsa
NASA Langley Research Center
Hampton, Virginia

[redacted]ITE-VOLUME FORMULATION

The integral form of the conservation laws for mass, momentum, and energy is given in equation (1). The solution vector

$$W = \left[\rho,\ \rho u,\ \rho v,\ \rho E\right]^T,$$

where ρ, (u,v), and E denote the density, Cartesian velocity components, and total internal energy, respectively. The quantities F and G are flux vectors. The variables x and y are Cartesian coordinates, and t represents time. In equation (1), Ω denotes the region of interest and $\partial\Omega$ is the boundary curve. If the computational region is partitioned with quadrilaterals and equation (1) is applied to each one, a system of ordinary differential equations is obtained. One of these equations is given in the figure. The quantity S is the area of the cell being considered. The vector W is evaluated at the cell center, and the indices i and j identify the cell.

$$\frac{\partial}{\partial t}\iint_{\Omega} W\,dx\,dy + \int_{\partial\Omega}(F\,dy - G\,dx) = 0 \qquad (1)$$

Applying Eq. (1) to the quadrilateral ABCD

$$\frac{d}{dt}\left(S_{ij}W_{ij}\right) + \left(H_{AB} + H_{BC} + H_{CD} + H_{DA}\right) = 0$$

where

$H_{AB}, H_{BC}, H_{CD}, H_{DA}$ -- fluxes through sides of cell

FINITE-VOLUME MESH

The fluxes H_{AB}, H_{BC}, H_{CD}, H_{DA}, in the case of the momentum equations, account for momentum flow into and out of a cell by convection and by molecular transport. If the thin-layer Navier-Stokes equations are considered, viscous fluxes are included in only H_{BC} and H_{DA}. Consider cell face BC. The viscous stresses at this face are determined by applying Green's theorem to cell A'B'C'D'. In a similar manner, the viscous stresses at cell face DA are obtained.

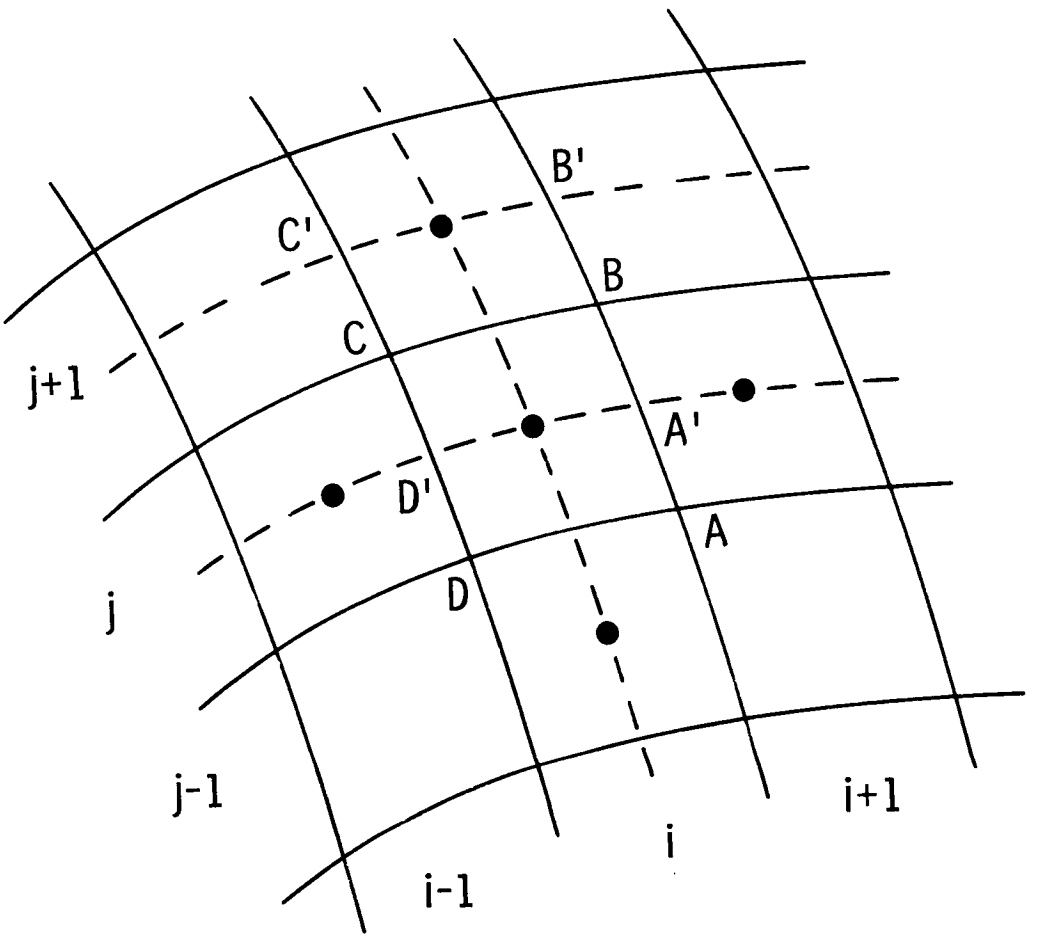

NUMERICAL PROCEDURE

In this figure, the basic elements of the present procedure for the numerical solution of the thin-layer Navier-Stokes equations are given. A modified four-stage Runge-Kutta scheme is used to advance the solution in time. Artificial dissipation terms are added to the difference equations, and they are third order in smooth regions of the flow field. These terms are included for several reasons: (1) to enhance the coupling of the difference equations, (2) to control nonlinear instabilities, and (3) to eliminate oscillations at shock waves. Three techniques are employed to accelerate convergence to steady state. With local time stepping, the solution at any point in the domain is advanced at the maximum time step allowed by stability. This results in faster signal propagation and thus faster convergence. Enthalpy damping involves, in general, adding damping terms to the flow equations that are proportional to the difference between the local total enthalpy and the free-stream value. These terms vanish at steady state. Finally, residual smoothing is an implicit procedure to extend the local stability range.

- Modified four-stage Runge-Kutta scheme
- Artificial dissipation terms added (blending of 2nd and 4th differences)
- Acceleration techniques
  - (1) Local time stepping
  - (2) Enthalpy damping
  - (3) Residual smoothing--extend stability range

NUMERICAL PROCEDURE

The computer code for the scheme is vectorized for efficient processing. The algebraic method of LeBalleur (ref. 1) is used to construct C-type meshes for airfoil calculations. The algebraic eddy viscosity model of Baldwin and Lomax (ref. 1) is employed for turbulence closure.

- Computing efficiency enhancement -- vectorization of scheme
- Algebraic mesh generation -- C-type for airfoils
- Algebraic turbulence model -- Baldwin-Lomax

FOUR-STAGE TIME-STEPPING SCHEME

The four-stage scheme presented in the figure is used to integrate the flow equations in time. The quantities R, L, and D are spatial discretization operators. The operator L is associated with convection, and the operator D is associated with the physical viscous terms and artificial dissipation terms. The terms of D operating on W are evaluated at the first stage and frozen for the remaining stages. For the given values of α_i (i = 1,2,3), this scheme is second-order accurate in time for nonlinear problems. The advantage of the modified scheme over the standard Runge-Kutta scheme is that it requires less array storage in computer processing (an important consideration for three-dimensional problems). Central difference operators are employed for the spatial derivatives in the flow equations. The scheme is second-order accurate in space for sufficiently smooth grids.

$$W^{(1)} = W^n - \alpha_1 \Delta t R W^n$$

$$W^{(2)} = W^n - \alpha_2 \Delta t R W^{(1)}$$

$$W^{(3)} = W^n - \alpha_3 \Delta t R W^{(2)}$$

$$W^{(4)} = W^{n+1} = W^n - \Delta t R W^{(3)}$$

where on the (q + 1) st stage

$$RW^{(q)} = \frac{1}{S}\left(LW^{(q)} - DW^n\right)$$

and

$$\alpha_1 = 1/4, \quad \alpha_2 = 1/3, \quad \alpha_3 = 1/2$$

ENTHALPY DAMPING

In the present work, a damping term is added to the energy equation only. Note that in the absence of viscous terms, the total enthalpy (H) is constant throughout the flow field if there is a uniform free stream. In the case of viscous flows, constant H can be a solution of the energy equation. Moreover, if the dominant viscous terms (boundary-layer type approximations) are retained in the flow equations, the equation at the bottom of the figure is obtained. Then, if the Prandtl number is unity and the solid boundaries are adiabatic, constant H is a solution of the energy equation. With similar assumptions, the total enthalpy can be shown to be constant for turbulent flows. As indicated previously, enthalpy damping can accelerate convergence. It is especially helpful during the initial time steps of a calculation. At the present time, we are investigating other forms of damping so as to not preclude the capability to solve problems where heat-transfer effects are important.

Consider the energy equation

$$\frac{\partial}{\partial t}(\rho E) + \frac{\partial}{\partial x}(\rho u H) + \frac{\partial}{\partial y}(\rho v H) + \underbrace{\alpha\rho\,(H - H_\infty)}_{\text{damping term}} = \text{viscous terms} \qquad (1)$$

Retaining the dominant viscous terms, we obtain for laminar flow

$$\text{LHS (1)} = \frac{\partial}{\partial y}\left\{\frac{\mu}{Pr}\left[\frac{\partial}{\partial y}(H) + (Pr - 1)\,\frac{\partial}{\partial y}\left(\frac{u^2}{2}\right)\right]\right\}$$

RESIDUAL SMOOTHING

In this figure, some details of implicit residual smoothing are examined. A two-step scheme is considered. The quantity L is the spatial discretization operator. If residual smoothing is applied to the second stage, the factored form given in the figure is used. In this equation, the product symbol is taken over the number of spatial dimensions (ℓ), β is the smoothing parameter, and δ_{XX} is the standard central difference operator. The quantities $\left(u^{n+1} - u^n\right)$ and $\left(u^{(2)} - u^n\right)$ are the updated and explicit residuals, respectively. If β is sufficiently large, the scheme is unconditionally stable. However, as revealed through linear stability analyis, the fastest convergence to steady state is not realized with a very large time step.

Consider the two-step scheme

$$u^{(1)} = u^n - \alpha \Delta t L u^n$$

$$u^{(2)} = u^n - \Delta t L u^{(1)}$$

Residual smoothing for the second stage is given by

$$\prod_{\ell} \left(1 - \frac{\beta_\ell}{4} \delta_{xx}^{(\ell)}\right)\left(u^{n+1} - u^n\right) = u^{(2)} - u^n$$

where δ_{xx} is central difference operator.

COMPUTATIONAL DOMAIN FOR AIRFOIL CALCULATIONS

This figure shows a sketch of the computational domain for airfoil calculations. The outer boundary (ABC) is a C-type curve, and it reflects the type of mesh used.

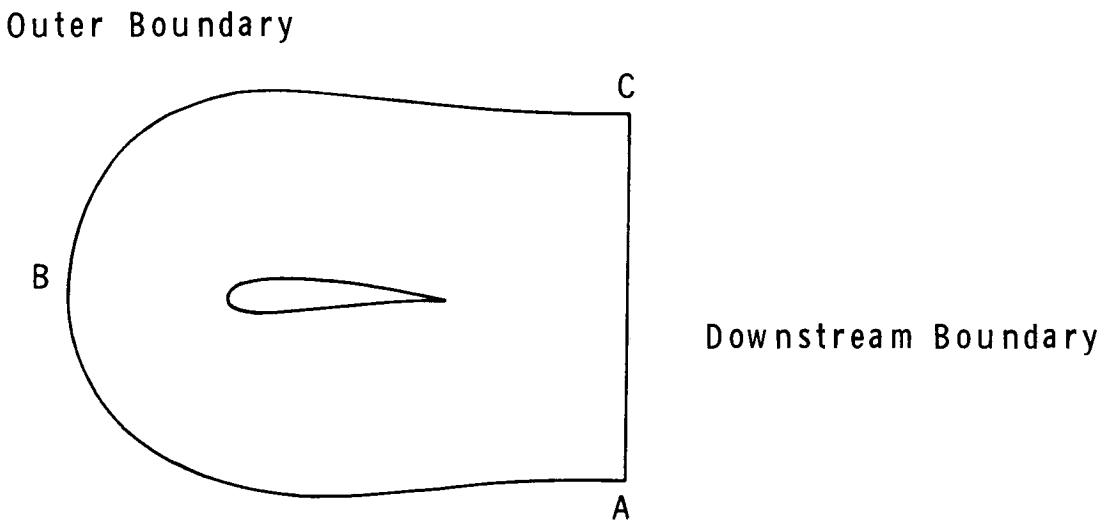

BOUNDARY CONDITIONS

During a calculation, a test is performed to determine if there is inflow or outflow at a given location along the outer boundary curve. If there is inflow, the total enthalpy H, entropy S, and tangential velocity component U are specified. If there is outflow, the Riemann invariant is specified. The quantities V, a, and γ are the normal velocity component, speed of sound, and specific heat ratio, respectively.

- SURFACE BOUNDARY
  - (1) No slip
  - (2) Adiabatic condition
- OUTER BOUNDARY
  - (1) Inflow--specify H, S, U
  - (2) Outflow--specify Riemann invariant

$$V - \frac{2a}{\gamma-1}$$

- DOWNSTREAM BOUNDARY--SPECIFY P

TURBULENT FLAT-PLATE FLOW

The Runge-Kutta time-stepping scheme was used to compute turbulent flow ($M_\infty = 0.5$, $Re_\infty = 10^6$) over a semi-infinite flat plate. In the figure on the left, the variation of the skin friction (based on free-stream conditions) with local Reynolds number is presented. The computed result is compared with an incompressible correlation. There is fairly good agreement except in the leading-edge region. Note that since the thin-layer Navier-Stokes equations were solved in the calculation, no attempt was made to resolve the leading-edge region of the plate. In the figure on the right, velocity profiles at X/L = 0.875 are compared. The present result agrees very well with that obtained with the implicit code of Steger (uses Beam and Warming scheme, ref. 1).

($M = 0.5$, $Re = 10^6$)

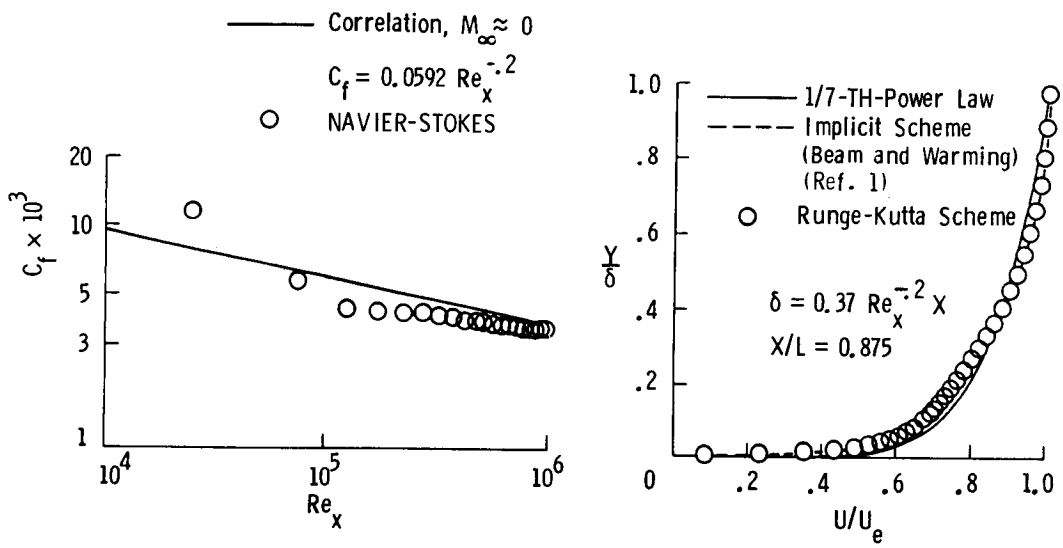

PARTIAL VIEW OF AIRFOIL GRID

This figure shows a partial view of a representative C-type grid used in airfoil calculations. There is grid clustering in the leading- and trailing-edge regions of the airfoil. In addition, there is fine mesh spacing adjacent to the airfoil surface in order to resolve the boundary layer.

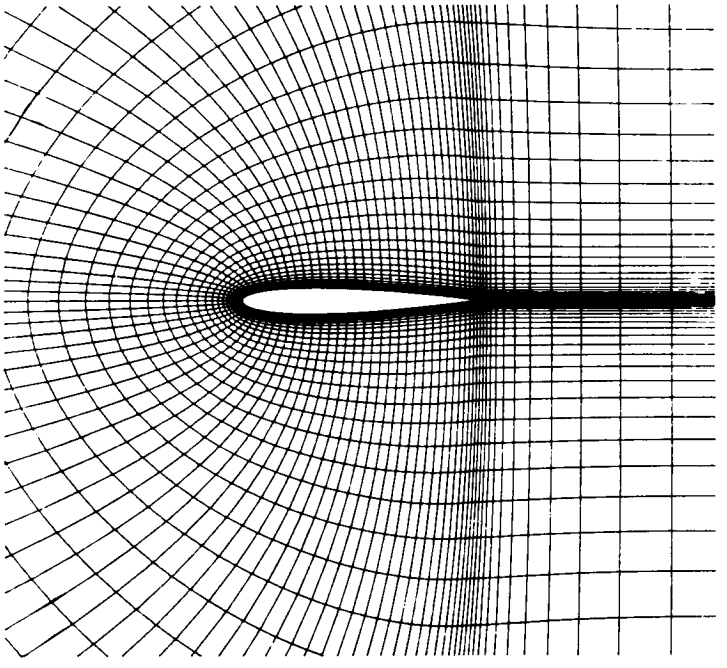

LAMINAR FLOW OVER AN NACA 0012 AIRFOIL

This figure shows results for laminar flow over an NACA 0012 airfoil. The free-stream Mach number and Reynolds number for this case are 0.5 and 5×10^3, respectively. In the figure on the left, the variation of pressure coefficient with nondimensional axial distance (X/C, where C is the airfoil chord) is presented. The viscous solution is compared with the inviscid solution. There are significant viscous effects in the leading- and trailing-edge regions. In the figure on the right, the computed skin-friction distribution is shown. Flow separation is indicated at the 0.82 chord location.

($M = 0.5$, $Re = 5\times10^3$, $\alpha = 0$)

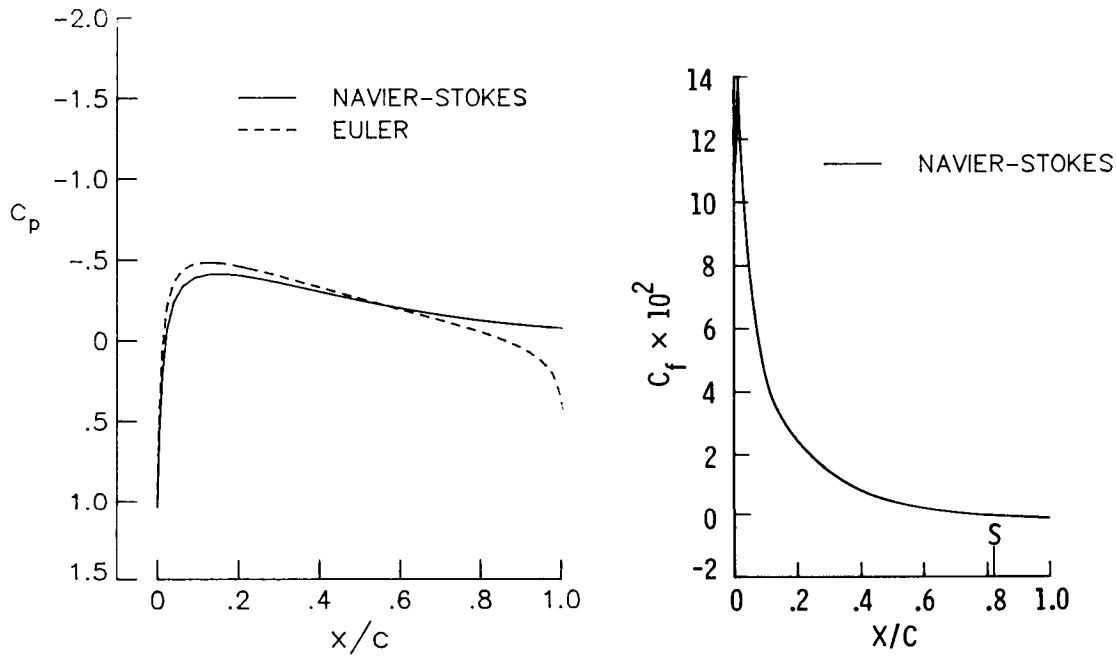

LAMINAR AIRFOIL FLOW---STREAMLINES

This figure shows the streamlines on the upper trailing-edge surface of the airfoil. The indicated separation bubble is thin and elongated. Since the velocities inside the bubble are small, accuracy of the solution is of special concern. Therefore, two calculations were done. In the first case, the grid consisted of 128 cells around the airfoil and 32 cells in the normal-like direction. In the second case, a 128×64 mesh was used. The cell spacing in the normal-like direction was half as large. The solutions were essentially the same except for the reverse flow region. This region was about 7 percent larger in longitudinal extent in the finer grid case.

$(M = 0.5, \quad Re = 5 \times 10^3, \quad \alpha = 0)$

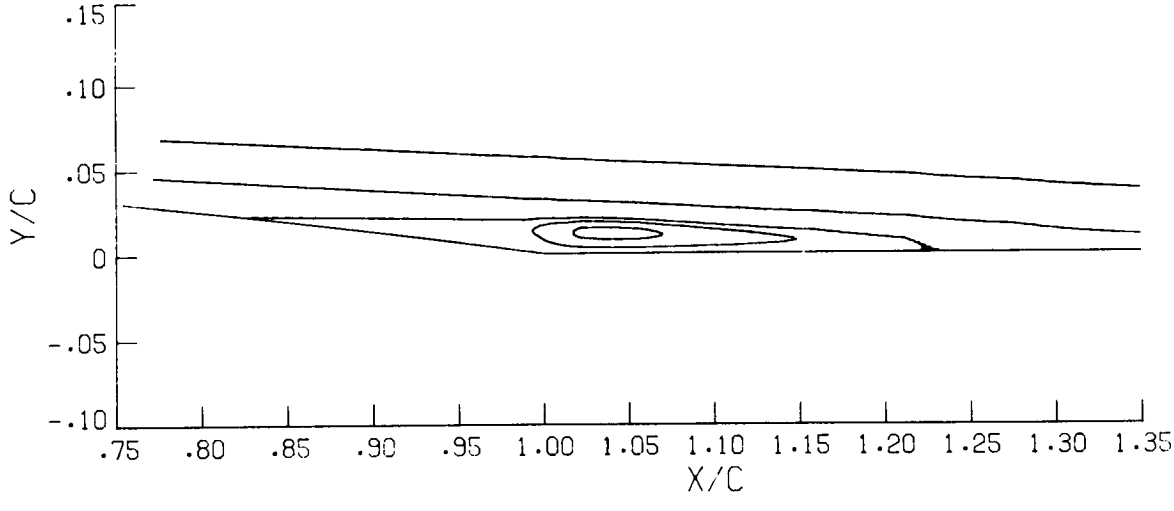

TURBULENT FLOW OVER AN NACA 0012 AIRFOIL

Pressure and skin-friction distributions for turbulent flow over an NACA 0012 airfoil ($M_\infty = 0.5$, $Re_\infty = 2.89\times10^6$) are presented in this figure. There is good agreement between the computed and experimental pressure distributions. In the figure on the right, the skin-friction distribution calculated with the present Navier-Stokes code is compared with that determined with a boundary-layer code. The mesh spacing at the surface in the boundary-layer calculation was more than an order of magnitude smaller than that used in the Navier-Stokes calculation. There is fairly good agreement between these solutions except in the immediate vicinity of the airfoil leading edge. The present solution probably does not have adequate resolution of the very thin turbulent boundary layer at the leading edge.

($M = 0.5$, $Re = 2.89\times10^6$, $\alpha = 0$)

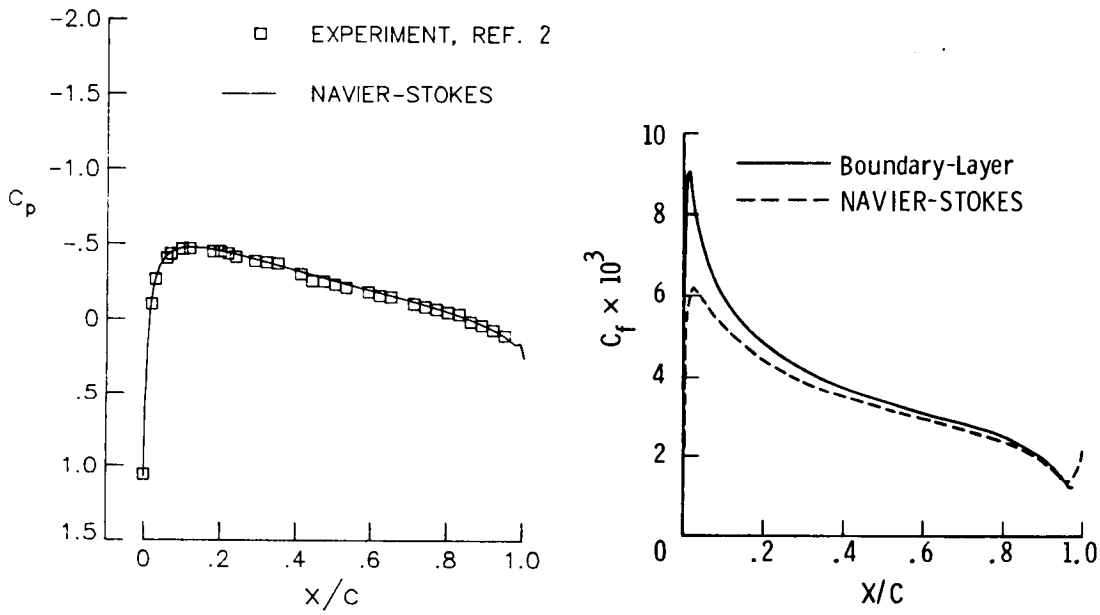

SUBSONIC FLOW OVER AN NACA 0012 AIRFOIL

In this figure, the predicted pressure distribution for subsonic viscous flow ($M_\infty = 0.5$, $Re_\infty = 2.93\times10^6$) over an NACA 0012 airfoil at angle of attack (3.51^o) is compared with that for inviscid flow and with experimental data. The angle of attack has been corrected for wind tunnel wall effects. There is good agreement between the present Navier-Stokes results and experiment. The influence of viscosity on this solution, in particular at the suction peak, is evident.

($M = 0.5$, $Re = 2.93\times10^6$, $\alpha = 3.51$)

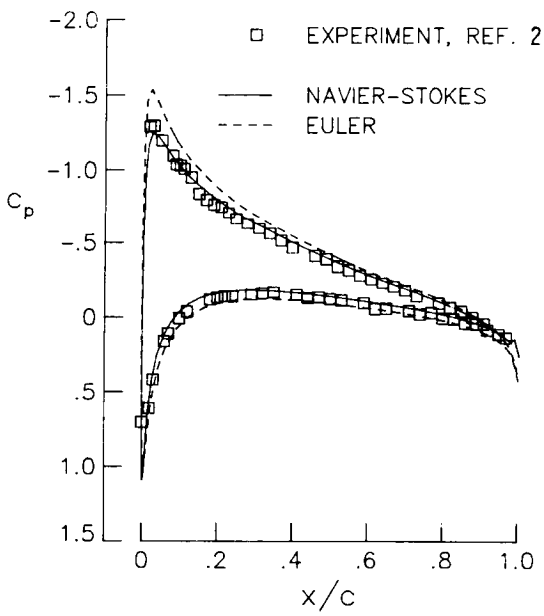

	C_L
EXP.	0.386
VISCOUS	0.388
INVISCID	0.429

TRANSONIC FLOW OVER AN NACA 0012 AIRFOIL

This figure presents pressure distributions for transonic flow ($M_\infty = 0.756$, $Re_\infty = 4.01\times10^6$) over an NACA 0012 airfoil. The results from the viscous and inviscid calculations show good agreement with the experimental data. The shock in this case is very weak, and this is evident in the Mach number contours in the next figure.

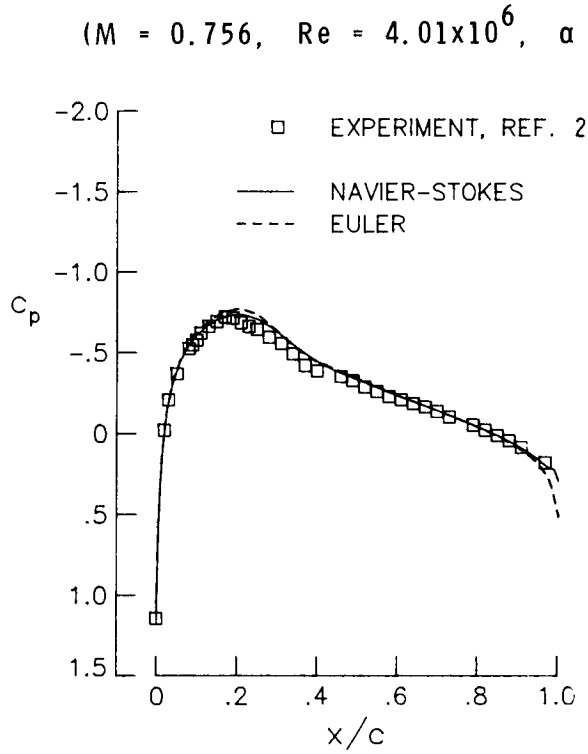

MACH NUMBER CONTOURS

The supersonic region is indicated in this figure.

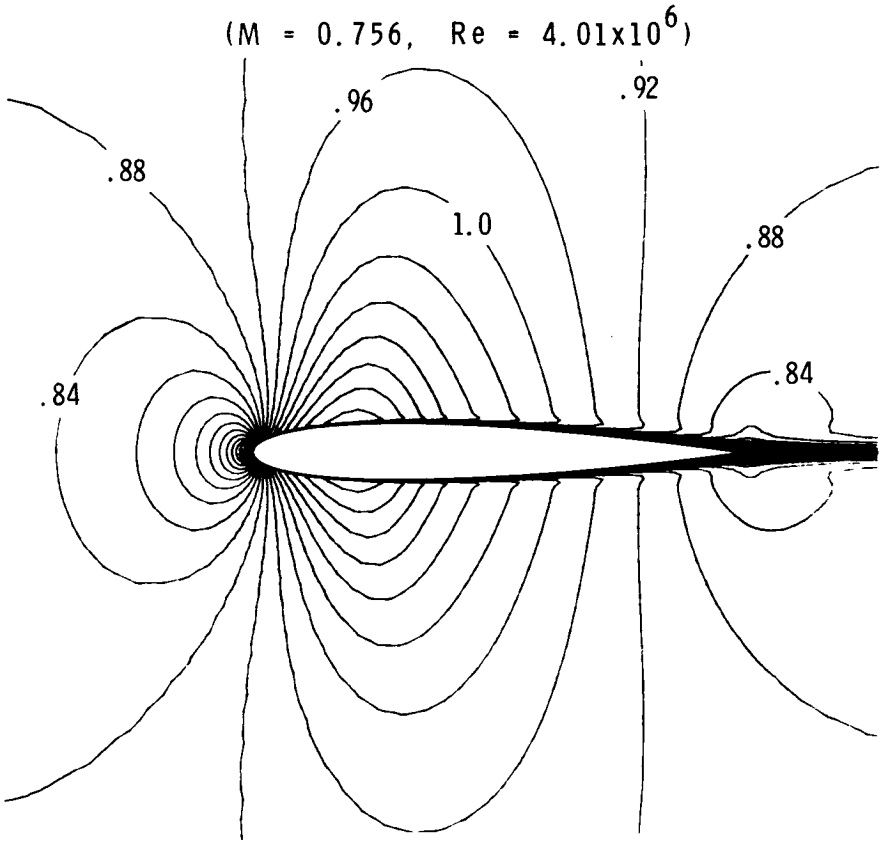

TRANSONIC FLOW OVER AN RAE 2822 AIRFOIL

This figure shows the pressure distribution for supercritical flow over an RAE 2822 airfoil. The free-stream Mach number and Reynolds number are 0.730 and 6.5×10^6, respectively. The wind tunnel corrected angle of attack is 2.79°. Transition of the boundary layer was fixed at the experimental value of 3-percent chord. In this calculation, a C-type grid with 260 cells around the airfoil and 96 cells in the normal-like direction was used. There is good agreement between the computed and experimental pressure distributions. The predicted lift and drag coefficients are also compared with those of the experiment.

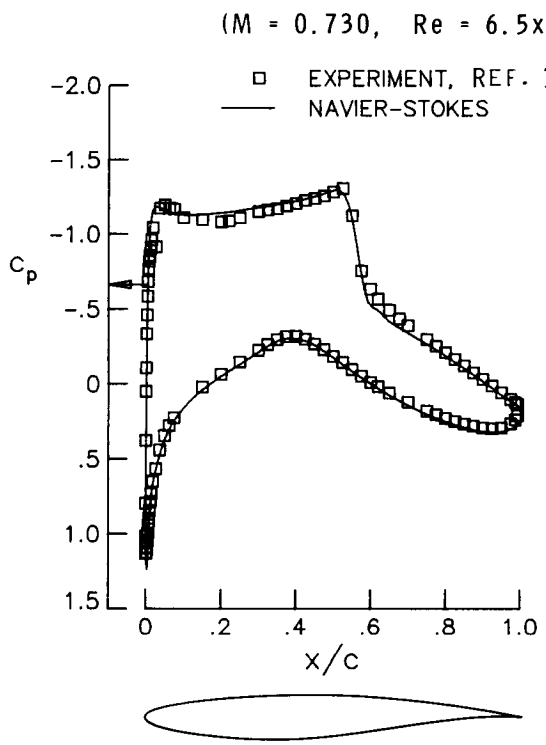

	C_L	C_D
EXP.	0.803	0.0168
VISCOUS CALC.	0.820	0.0193

UPPER SURFACE SKIN FRICTION FOR RAE 2822 AIRFOIL

This figure presents a comparison of the calculated and experimental skin-friction distributions. The skin-friction coefficient is based on boundary-layer edge conditions. In general, there is fairly good agreement with the experimental data. However, the computation shows a small shock-induced separation bubble and incipient trailing-edge separation, which are not indicated by the experimental data. The present computed result is generally consistent with those of other investigators. The predicted rise in skin friction at the airfoil trailing edge is probably due to inadequate representation by the basic Baldwin-Lomax algebraic eddy viscosity model of the transition from the wall boundary layer to the free shear layer.

($M = 0.730$, $Re = 6.5 \times 10^6$, $\alpha = 2.79$)

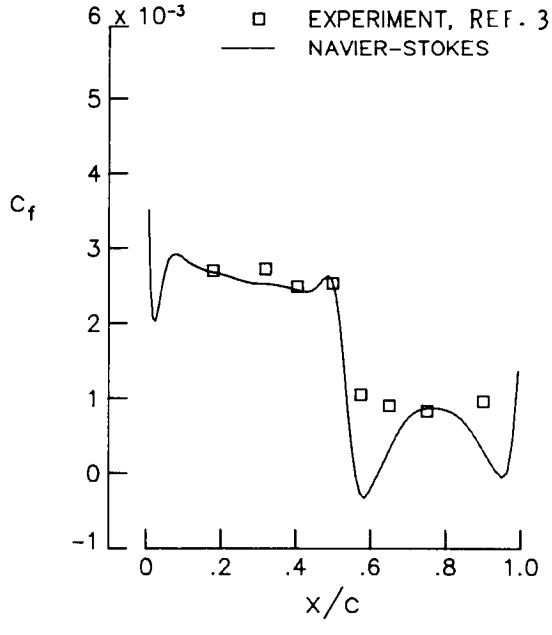

CONVERGENCE HISTORIES FOR LAMINAR AIRFOIL FLOW

This figure displays variations of the common logarithm of the root mean square of the residual of the continity equation with the number of time steps. Curve A shows the residual decay when enthalpy damping is added to the Runge-Kutta time-stepping scheme. Curve B indicates the improvement in the convergence rate with the inclusion of implicit residual smoothing. Satisfactory convergence for engineering applications is achieved in 1,300 time steps, which corresponds to 2.5 minutes on the Vector Processing System (VPS) 32 at Langley Research Center.

($M = 0.5$, $Re = 5 \times 10^3$, $\alpha = 0$, 128x32 GRID)

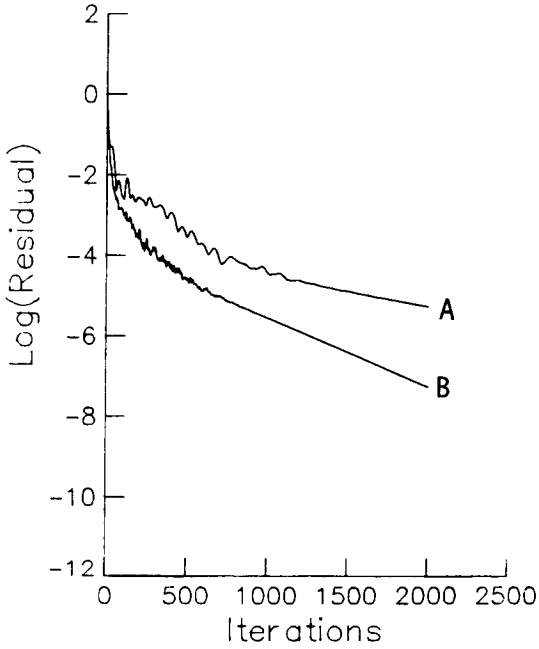

A---enthalpy damping

B---enthalpy damping and residual smoothing

CONVERGENCE HISTORIES FOR TURBULENT AIRFOIL FLOW

The figure on the left shows the convergence history when only local time stepping is employed to accelerate convergence. This convergence history is highly oscillatory. In the figure on the right, the convergence behavior for a computation using enthalpy damping and residual smoothing is much more monotonic. For this case, acceptable convergence is realized in about 1,250 time steps (4 minutes on the VPS-32). Note that the present computer code is not optimized for the VPS-32 system. With optimization the computer processing times can be reduced by a factor of 2 to 3. In conclusion, the final rate of reduction of the residual for the turbulent flow cases can be quite slow. Based on previous work with Euler equations, significant improvement in this rate appears to be possible with a multigrid scheme. At the present time, this is being investigated.

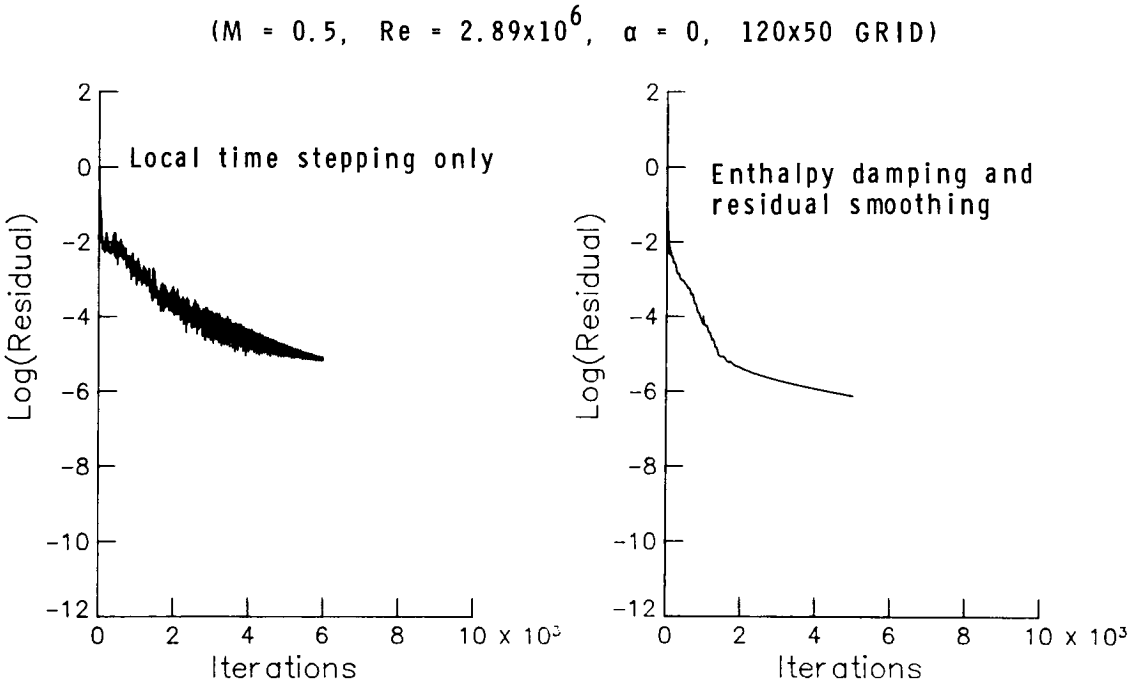

THIN-LAYER NAVIER-STOKES (LAMINAR) SOLUTIONS FOR INFINITE RECTANGULAR WING

In this figure, the velocity profiles computed from two- and three-dimensional thin-layer Navier-Stokes codes are compared at selected axial locations for an infinite, rectangular wing. The wing is constructed with constant chord NACA 0012 airfoil sections. Numerical solutions for this configuration were obtained at $M_\infty = 0.5$ and $Re_c = 5000$. A 96×32 C-grid at each spanwise station was employed, and a total of four spanwise stations were used for the three-dimensional calculations. As expected, the solutions at each spanwise station were identical; and, as indicated by the results shown in this figure, these are in excellent agreement with the solutions obtained from two-dimensional analysis.

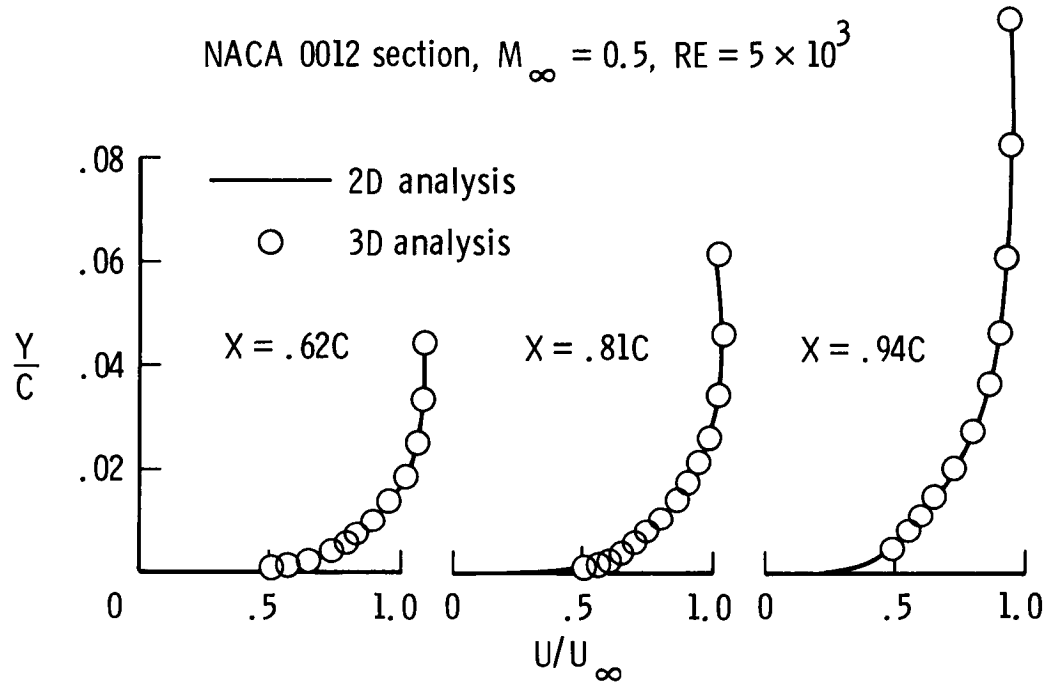

THIN-LAYER NAVIER-STOKES (TURBULENT) SOLUTIONS FOR INFINITE RECTANGULAR WING

The configuration selected for the results shown in this figure is identical to the one shown in the previous figure. However, the flow here is assumed to be fully turbulent and the Reynolds number is taken to be 2.89×10^6. A 120×50 C-grid was employed in each cross section for these calculations. Again, the results from the two- and three-dimensional analyses are found to be in excellent agreement.

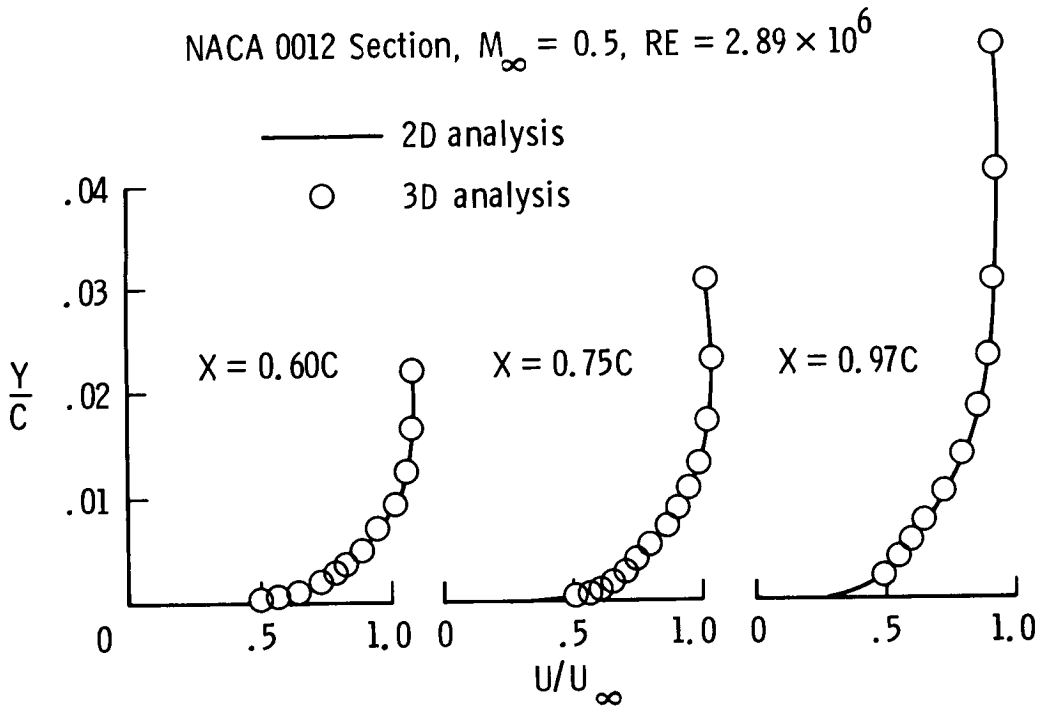

PARTIAL VIEW OF GRID EMPLOYED FOR WING CALCULATIONS

A partial view of a typical grid employed for wing calculations is shown in this figure. A C-H type grid topology is employed here; i.e., sections of C-type grids are stacked at various spanwise stations. Strong grid-clustering is employed near the wing surface to resolve extremely thin turbulent boundary layers that develop at high Reynolds numbers. The grid is also clustered near leading- and trailing-edge regions of the airfoil. A 121×51×17 grid is selected for an initial set of calculations.

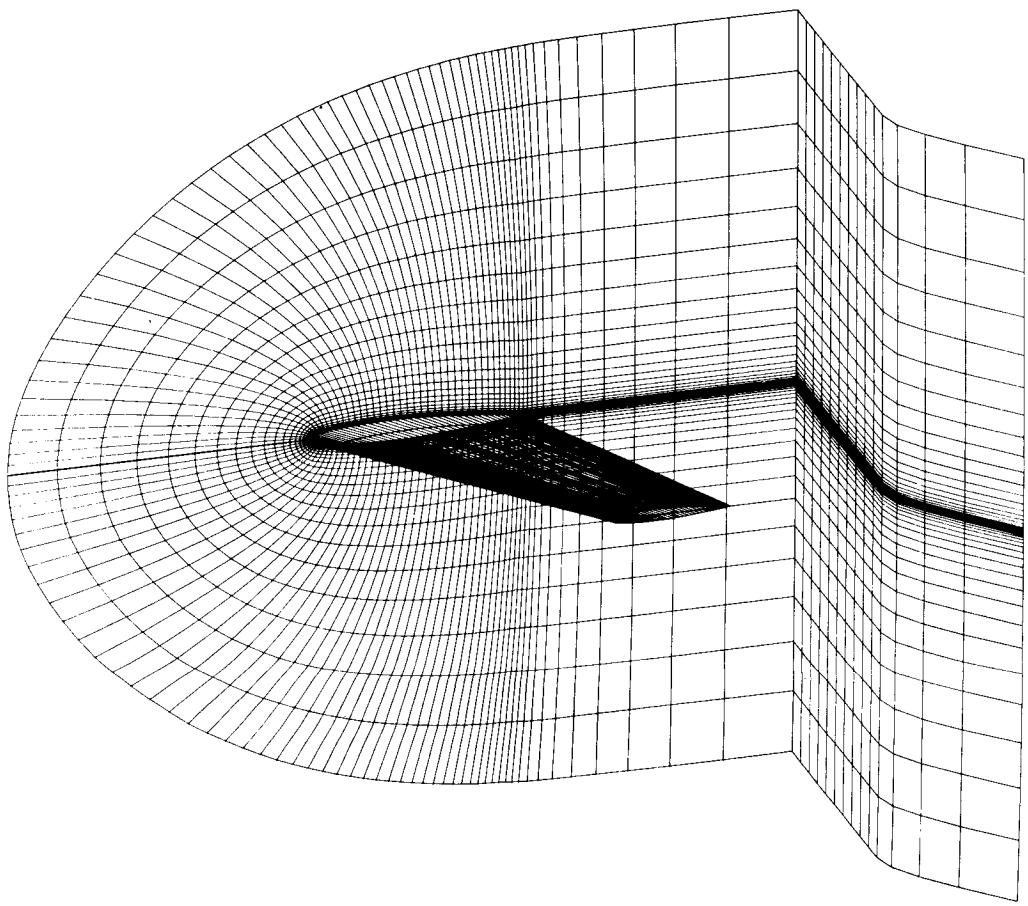

CONCLUDING REMARKS

A finite-volume scheme for numerical integration of the Euler equations has been extended to allow solution of the thin-layer Navier-Stokes equations in two and three dimensions. The extended algorithm, which is based on a class of four-stage Runge-Kutta time-stepping schemes, has been made numerically efficient through the following convergence acceleration techniques: (1) local time stepping, (2) enthalpy damping, and (3) residual smoothing. Also, the high degree of vectorization possible with the algorithm has yielded an efficient program for vector processors. The scheme has been evaluated by solving laminar and turbulent flows. Numerical results have compared well with either theoretical or other numerical solutions and/or experimental data.

- Algorithm for Navier-Stokes equations constructed from a class of explicit multistage time-stepping schemes
- Flexibility in treating arbitrary geometries obtained with a finite-volume formulation
- Numerical efficiency achieved by acceleration techniques
- Computer processing enhanced through vectorization
- Scheme evaluated by solving laminar and turbulent flows

REFERENCES

1. Swanson, R. C.; and Turkel, Eli: A Multistage Time-Stepping Scheme for the Navier-Stokes Equations. NASA CR-172527, Feb. 1985.

2. Thibert, J. J., Granjacques, M., and Ohman, L. H.: NACA 0012 Airfoil. AGARD Advisory Report No. 138, Experimental Data Base for Computer Program Assessment, May 1979.

3. Cook, P. H., McDonald, M. A., and Firmin, M. C. P.: Aerofoil RAE 2822 - Pressure Distributions, and Boundary Layer and Wake Measurements. AGARD Advisory Report No. 138, Experimental Data Base for Computer Program Assessment, May 1979.